

Predicting the Geothermal Gradient in Colombia: a Machine Learning Approach

Juan C. Mejía-Fragoso^{1*}, Manuel A. Flórez¹ and
Rocío Bernal-Olaya¹

¹Universidad Industrial de Santander, Carrera 27 Calle 9, Bucaramanga,
680002, Santander, Colombia.

*Corresponding author(s). E-mail(s): juan.mejia3@correo.uis.edu.co;
Contributing authors: maflotor@uis.edu.co; rbernal@uis.edu.co;

Abstract

Accurate determination of the geothermal gradient is critical for assessing the geothermal energy potential of a given region. Of particular interest is the case of Colombia, a country with abundant geothermal resources. A history of active oil and gas exploration and production has left drilled boreholes in different geological settings, providing direct measurements of the geothermal gradient. Unfortunately, large regions of the country where geothermal resources might exist lack such measurements. Indirect geophysical measurements are costly and difficult to perform on regional scales. Computational thermal models could be constructed, but they require very detailed knowledge of the underlying geology and uniform sampling of subsurface temperatures to be well-constrained. We present an alternative approach that leverages recent advances in supervised machine learning and available direct measurements to predict the geothermal gradient in regions where only global-scale geophysical datasets and coarse geological knowledge are available. We find that a Gradient-Boosted Regression Tree algorithm yields optimal predictions and extensively validates the trained model. We show that the predictions of our model are within 12% accuracy and that the independent measurements performed by other authors agree well with our model. Finally, we present a geothermal gradient map for Colombia that highlights regions where further exploration and data collection should be performed.

Keywords: Geothermal Energy, Machine Learning, Colombia, Geothermal Gradient, Prediction

1 Highlights

- A machine learning approach for geothermal gradient prediction using only global-scale geophysical datasets and low-resolution geological maps.
- Model predictions show good agreement with independent measurements and high accuracy.
- The model allows for the generation of a new geothermal gradient map of Colombia highlighting the potential of unexplored regions.
- Model predictions follow regional trends established by prior geological knowledge.
- Model predictions confirm high geothermal gradients in the Amazon, an unexplored region, giving a baseline for studying the area.

2 Introduction

The tectonic and geological characteristics of Colombia give rise to thermal anomalies and regions exhibiting elevated geothermal gradients, which represent promising sources of geothermal energy. However, performing accurate estimations of the country’s potential for geothermal energy generation remains challenging. The most current geothermal gradient map for Colombia covers roughly half of the country’s territory (Alfaro et al., 2009), for the rest no systematic determinations of the geothermal gradient are available. Some studies have tried to address this issue. Uyeda and Watanabe (1970) observed normal to subnormal geothermal gradient values across South America, with higher values in the Andes related to geothermal activity. Bachu et al. (1995) focused on the Llanos Basin, finding that geothermal gradients decrease with depth and westward. In northwestern Colombia, Quintero et al. (2019) estimated geothermal gradients using grid systems and aeromagnetic data. Unfortunately, all of these studies are either focused on narrow areas of interest or scales that are too large for meaningful estimations of the country’s geothermal potential. Measurements from boreholes drilled by the oil and gas industry provide the best direct constraint on the geothermal gradient; in the case of Colombia, they are either very sparse or clustered to specific regions, as the need to decarbonize the economy grows, it is unlikely that the past pace of oil exploration activity will continue. Therefore, a different approach is needed if Colombia is to realize its clean energy production objectives (Alfaro et al., 2021).

It is seldom impossible to develop comprehensive geothermal gradient models for an entire country using only direct borehole measurements (Burton-Johnson et al., 2020), so indirect approaches are necessary. Geophysical methods provide complementary estimates of the geothermal gradient over large spatial scales and depths that are inaccessible by boreholes alone; magnetic and electrical surveys exploit the thermal properties of rocks to estimate temperature gradients. While ideal, due to their cost, such surveys are typically performed once a narrow target of interest has been identified. Numerical thermal modeling has emerged as a useful tool for estimating geothermal gradients as it allows for the prediction of the entire temperature field of the region’s subsurface (Békési et al., 2020). Thermal models require detailed knowledge of the underlying geology, direct temperature and heat flow measurements and involve a significant number of assumptions. For Colombia, while in principle modeling could be performed, it is unlikely to yield accurate results.

Data-driven approaches have become viable alternatives for the estimation of the earth’s thermal properties. Goutorbe et al. (2011) explored empirical estimators to estimate heat flow in data-scarce regions, using global geological and geophysical proxies; obtaining results that demonstrate their effectiveness in approximating heat flow. Lucazeau (2019) updates the global terrestrial heat flow dataset with around 70,000 measurements, finding that Earth’s total heat loss is approximately 40–42 TW, closely matching previous conductive cooling estimates. The study highlights improved measurement quality and coverage, especially in young oceanic regions, which significantly reduce discrepancies with existing models.

Rezvanbehbahani et al. (2017) used a gradient boosting regression tree algorithm and a catalog of global geological features to produce a new geothermal heat flow (GHF) map of Greenland, their predictions were consistent with regional geology, tectonics and ice core measurements. A similar approach was used to predict GHF in Antarctica by Lösing & Ebbing (2021), it incorporated regional datasets to improve predictions. Matiz-León (2023) emphasized the importance of statistical methods and spatial prediction for estimating geothermal gradients, especially in areas lacking in-situ data. Advances in machine learning and the increasing availability of regional and global geological datasets allow for the development of cost effective approaches to provide initial baselines of the thermal properties of entire countries.

Machine learning has increasingly been used in many geothermal-related studies as well. Assouline et al. (2019) proposed a methodology to extract the very shallow geothermal potential at a national scale for Switzerland, using a combination of geographic information systems, traditional modeling, and machine learning; this approach leverages data such as monthly temperatures at various depths in the surface layer, along with thermal conductivity and diffusivity. Siler et al. (2021) applied unsupervised machine learning to identify key geological factors influencing geothermal production in Nevada’s Brady geothermal field, by analyzing geological data to discern controls on geothermal fluid pathways. Additionally, Pang et al. (2023) optimized machine learning algorithms to predict thermal conductivity (TC) using accessible, high-resolution logging data, employing techniques including random forest (RF), convolutional neural network (CNN), support vector regression (SVR), and particle swarm optimization-enhanced SVR (PSO-SVR). Furthermore, Alqahtani et al. (2023) leveraged borehole temperature and remote sensing data to pinpoint prospective zones with significant geothermal activity within the Harrat Rahat volcanic field in western Saudi Arabia, favoring exploration and drilling efforts.

In this work we present a Gradient Boosted Regression Tree algorithm to accurately predict the spatial distribution of geothermal gradients across a region. The approach only requires global scale geological and geophysical datasets, coarse geological knowledge and sparsely distributed borehole temperature measurements to produce accurate results. The paper is organized as follows: In section 4 we describe the details of the algorithm, in section 5 we present the data and the strategy used to train the model, in section 6 we provide extensive validation of our model and present a new map of geothermal gradients for Colombia. The predicted map highlights regions displaying relatively high geothermal gradients, where future exploration surveys should

be conducted. Further validation of the model is provided by the fact that the predictions show good agreement with indirect geophysical measurements of the geothermal gradient performed in the Amazon.

3 Geological Setting of Colombia

Colombia, positioned at the intersection of the Nazca, South American, and Caribbean plates, has a dynamic geological evolution extending back to 1780 million years. This dynamism is characterized by the Andean orogeny—still active today—along with significant faulting and seismic activity (Figure 1). The country’s structure comprises 12 tectonostratigraphic terranes, each with distinct geological features ranging from ancient gneisses and schists of the Mitú migmatitic complex to a variety of sedimentary sequences, igneous complexes, and quaternary deposits (Lobo, 1987). Colombia is located within the Pacific Ring of Fire, which encompasses a series of privileged regions for the generation of a geothermal energy and, therefore, is privileged with regions high geothermal activity, with 13 active volcanoes and a high presence of hot springs (Figure 2a) underscoring its significant geothermal potential (Clavijo et al., 2008; Marzolf, 2014).

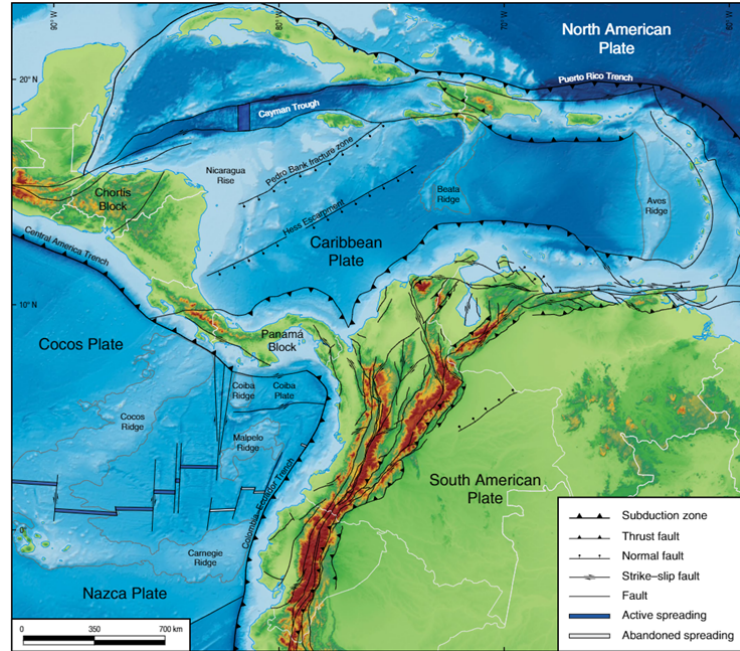


Fig. 1: Tectonic scheme of northern South America and the Caribbean. Taken from Gómez et al. (2020).

Colombian volcanism, predominantly associated with the uplift of the Central Cordillera, has shaped the nation’s landscape. The Upper Pliocene Andean Orogeny,

which occurred 4.5 to 3 million years ago, spurred extensive andesitic volcanism. This activity is aligned with the Palestina fault and is evident in the south of the Western Cordillera and into Panama. Furthermore, the Sinú fold belt—from the Gulf of Urabá to Galerazamba—displays a history of synsedimentary volcanism and magmatism marked by numerous volcanoes and mud diapirs (Lobo, 1987). Today, sedimentary volcanism is evidenced along the Caribbean coast and its platforms, notably through the mud volcanoes at Los Córdoba, Arboletes, Galerazamba, and others. The continued tectonic activity of the Andean region is manifest in frequent earthquakes and tremors.

The geological complexity of Colombia is further demonstrated by the existence of 23 marine and continental sedimentary basins, reflecting a rich tapestry of geological history and underscoring the potential for natural resource exploration and extraction within its borders (Gómez et al., 2020) (Figure 2b). The Upper Magdalena Valley, for instance, is a critical region for hydrocarbon extraction, harboring considerable deposits of oil and gas within the Cretaceous formations along the Eastern Cordillera. Similarly, the Middle Magdalena Valley is renowned for the intricate interaction of tectonic forces and sedimentation patterns that render it a hub for both scientific research and resource exploitation.

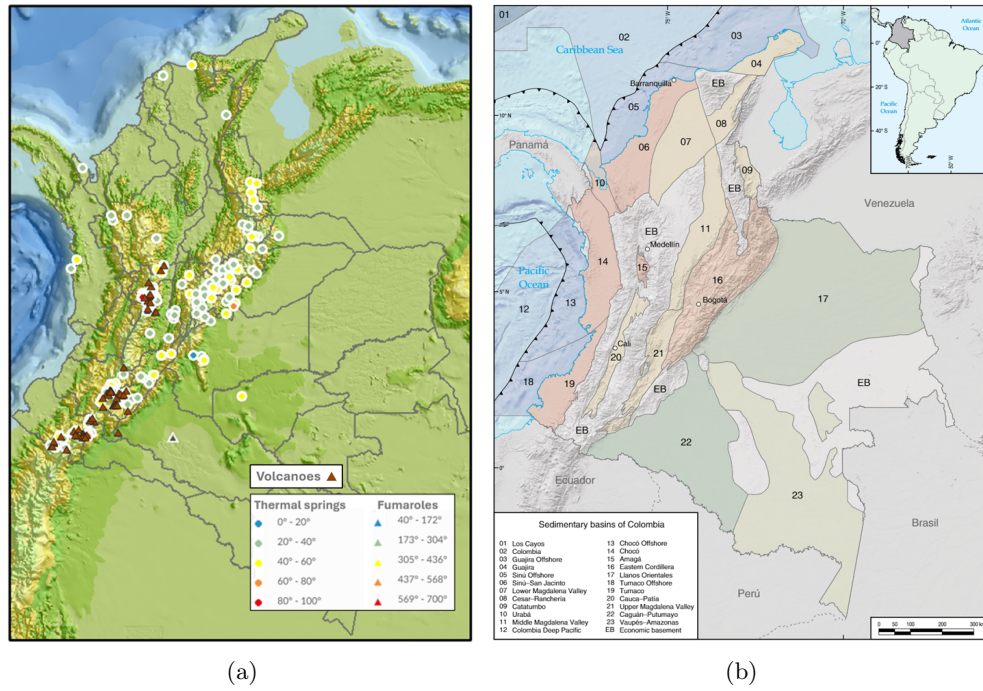


Fig. 2: (a) Thermal manifestations of Colombia and their temperature in degrees celsius. Source: sgc.gov.co/invtermaleas. (b) Sedimentary basins of Colombia. Taken from Gómez et al. (2020)

In contrast, the Llanos Basin, sprawling across the eastern plains, is characterized by Paleozoic and Cretaceous sedimentary layers. This basin is essential for its oil reserves, forming the cornerstone of the Colombian petroleum sector, and harboring the first geothermal energy pilot projects. In the maritime domain, the Caribbean and Pacific basins represent areas of untapped potential, with recent explorations indicating significant possibilities for oil discoveries, marking new horizons for hydrocarbon exploration. The Amazon Basin (Amazonas-Vaupés) lies over a Precambrian foundation, followed by Paleozoic and Mesozoic strata, with a huge cover of neogene sedimentary rocks. Despite being largely unexplored due to its dense rainforest cover, the basin's geological kinship with hydrocarbon-rich Andean counterparts suggests latent resource potential, meriting cautious yet insightful exploration.

Colombia's detailed geological structure, spanning from the Andean Cordillera to the coastal and insular zones, brings a diversity of settings for energy and resource exploration. The diversity of rock types, from the archaic metamorphic rocks of the Guiana Shield in the east to the volcanic and sedimentary formations of the Andean regions, and the contemporary alluvial and marine deposits along the shores, illustrates a nation whose geodynamic context is favorable for a wide array of geological phenomena and resource deposits. A detailed geological map of Colombia can be seen in Figure 3.

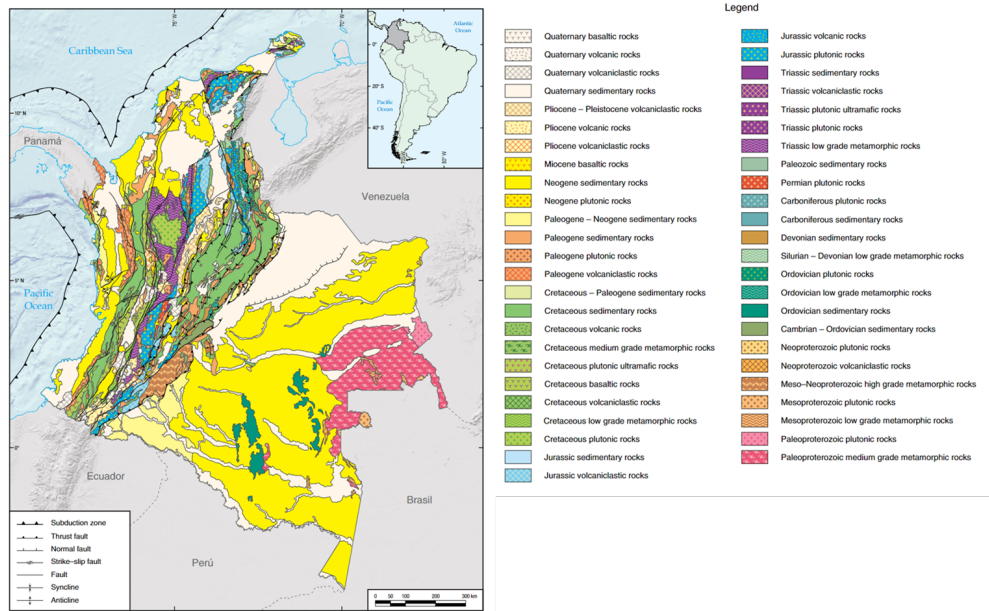


Fig. 3: Geological map of Colombia. Taken from Gómez et al. (2020).

4 Method

To achieve precise quantitative predictions within the geothermal context, it is necessary to utilize a regression algorithm that can effectively capture the relationship between the Geothermal Gradient and its geological setting. Our approach utilizes gradient boosting regression, a technique within the domain of supervised machine learning. This method systematically develops an ensemble of regression trees, where each tree is designed to incrementally adjust to the gradient of the loss function from the previous one, following the methodology outlined by Friedman (2001).

Regression trees are particularly adept at identifying complex non-linear relationships by recursively partitioning data based on specific criteria, such as maximum depth, number of leaves, and minimum samples per leaf. In the gradient-boosting framework, each iteration involves training a new tree on a subset of the data to accurately predict gradient descent steps. By aggregating these trees into an ensemble model, we improve our ability to predict outcomes for new data samples. This method stands out for its straightforward interpretability and operational simplicity, qualities that are often highlighted in the literature (Lösing & Ebbing, 2021).

We considered several machine learning algorithms, including Random Forest Regression. Our decision to utilize the Gradient Boosted Regression Tree algorithm was primarily influenced by its superior performance in terms of error metrics when compared to alternatives.

Specifically, the eXtreme Gradient Boosted Regression Tree, or XGBoost, operates on a sequential model building process where each successive tree is trained to correct the residuals of the previous ones. This method is particularly effective in complex datasets as it methodically minimizes errors and improves prediction accuracy over iterations. In contrast, Random Forest involves training multiple decision trees independently and averaging their predictions, which can be less effective in datasets where sequential error correction is beneficial.

The enhanced performance of XGradient Boosting in handling complex patterns and interactions within our dataset justified its selection over other methods such as Random Forest, despite the latter’s robustness and popularity in various applications.

4.1 Enhanced Gradient Boosting with XGBoost

The XGBoost algorithm, used in this study, is a refined version of gradient boosting regression Developed by Chen & Guestrin (2016), known for its high efficiency and robust regularization techniques. The methodology involving XGBoost encompasses the following aspects:

- **Objective Function:** XGBoost optimizes a comprehensive objective function that integrates both the loss function and regularization to mitigate overfitting and enhance model performance. The objective function is meticulously crafted as follows:

$$\mathcal{L}(\phi) = \sum_i l(\hat{y}_i, y_i) + \sum_k \Omega(f_k) \quad (1)$$

where $\mathcal{L}(\phi)$ represents the total loss to be minimized. The first term, $\sum_i l(\hat{y}_i, y_i)$, quantifies the prediction error through a loss function l , contrasting the predicted

outcomes \hat{y}_i against the actual targets y_i . The second term, $\sum_k \Omega(f_k)$, introduces regularization, encapsulating the complexity of the model to prevent overfitting. This dual approach ensures a balanced focus on achieving high predictive accuracy while maintaining model simplicity.

- **Regularization Component:** The regularization term $\Omega(f_k)$ plays a pivotal role in XGBoost’s formulation, explicitly designed to control model complexity:

$$\Omega(f_k) = \gamma T + \frac{1}{2} \lambda \|w\|^2 \quad (2)$$

Here, T signifies the total number of leaves in the tree k , and w denotes the vector of scores on the leaves. The parameter γ serves as the complexity cost assigned to each additional leaf, penalizing the growth of the tree structure. The term λ is the L2 regularization parameter on the leaf weights, reducing their magnitude to enhance generalization capabilities. Collectively, these components of $\Omega(f_k)$ ensure that the model remains both effective and interpretable.

- **Gradient and Hessian Optimization:** The optimization strategy in XGBoost employs the Newton-Raphson method, leveraging second-order derivatives for a refined adjustment of the model. The approximation for optimization at iteration t is given by:

$$\tilde{\mathcal{L}}(t) = \sum_{i=1}^n \left[g_i f_t(x_i) + \frac{1}{2} h_i f_t^2(x_i) \right] + \Omega(f_t) \quad (3)$$

In this equation, g_i and h_i represent the first and second-order gradients of the loss function with respect to the predictions, facilitating a nuanced understanding of the error landscape. This methodological choice allows XGBoost to more accurately pinpoint the direction and magnitude of model updates, markedly improving convergence speed and prediction accuracy.

- **Shrinkage and Column Subsampling:** Beyond regularization, XGBoost incorporates shrinkage and column subsampling to further enhance model robustness. Shrinkage, through the application of a learning rate, systematically scales down updates to the model, enabling more gradual learning and reducing the risk of overfitting. Column subsampling introduces randomness into the feature selection process for tree construction, promoting diversity among the trees and contributing to a more generalized model performance.

The implementation of XGBoost in our study uses these components to create a predictive model that is accurate and capable of handling the complexities inherent in geothermal gradient data.

4.2 Model Building and Evaluation

The development and validation phases of the model were structured to enhance its learning efficacy and accuracy in predicting geothermal gradients. Our methodological framework incorporates several critical steps that collectively improve the model’s performance.

The initial phase involved partitioning the data set into training and testing subsets with an 80/20 split, a standardized step for model construction, and subsequent validation with independent test data. This split facilitates the proper evaluation of the model’s ability to generalize. Furthermore, we performed hyperparameter optimization to fine-tune the XGBoost model, enhancing its predictive accuracy.

Following the hyperparameter tuning, the XGBoost model was trained using a squared error loss function. The training process incorporated a five-fold grid search approach to fine-tune parameters such as shrinkage, maximum tree depth, and sub-sampling rate. This iterative refinement ensured the robustness and adaptability of the model.

The validation of the model used a quantitative framework influenced by Lösing & Ebbing (2021) and Rezvanbehbahani et al. (2017), focusing on absolute and relative error metrics. For the assessment of the absolute error in the test set, we computed the mean square error (RMSE) and mean absolute error (MAE). Furthermore, normalized root mean square error (nRMSE) and normalized mean absolute error (nMAE) were calculated to provide standard and relative error measurements that are invariant to rescaling, facilitating comparative analysis.

The coefficient of determination, or R-squared (R^2), was calculated for both the test and training sets. The R^2 for the test set provides information on how well the predicted geothermal gradients align with the actual observed values, indicating the accuracy of the model in unseen data. Similarly, the R^2 value for the training set, referred to as the model score, reflects the proportion of variance in the geothermal gradient data that is predictable from the input variables, providing a gauge of the model’s efficacy during the learning phase.

Additionally, the process included analyzing the feature importance for each tree, averaged across the model. This analysis revealed how each feature reduced the uncertainty at its split point, weighted by the observation count in each node. These insights were crucial for improving the prediction model and understanding the factors that affect the predictions of geothermal gradients.

5 Data and features

In this section, we explain the data used to build our predictive model. The target feature y was the Apparent Geothermal Gradient (AGG) measurements from over 4000 well logs along the colombian territory, and for the predictor features X we use certain geological and geophysical features which are linked to each AGG value.

5.1 Apparent Geothermal Gradient

Colombian AGG measurements were taken from the Alfaro et al. (2009) Colombian Geothermal Gradients map, which includes the data from over 4000 wells (Figure 4a). The methodology they adopted for calculating the geothermal gradient for each well involved the following steps:

1. **Measurement of Bottom Hole Temperature (BHT):** BHT measurements from gas and oil wells were primarily used. These measurements represent the

maximum temperature recorded in a well. Due to the drilling process, these measurements are often lower than the actual formation temperature.

2. **Temperature Measurement Correction:** Various models and methods were used to correct for the effects of drilling on formation temperatures. The most widely used method for correcting BHT data was the AAPG method, which compares BHT measurements with equilibrium temperatures in wells in Louisiana and West Texas. The correction was achieved using a third-order polynomial equation, with BHT correction as a function of depth.
3. **Data Sources and Treatment:** Data were obtained from the Finder and LogDB tables supplied by EPIS. The organization of data involved forming pairs of depth-temperature data, and the selection process involved criteria for data quality. Units were converted from degrees Fahrenheit and feet to degrees Celsius and kilometers. Temperatures were corrected using the empirical method of AAPG.
4. **Estimation of Individual Well Gradients:** The maximum gradient within the upper crust was assumed to be vertical and calculated using the equation $G = \Delta T / \Delta P = (TBHT - T_s) / Z$, where $TBHT$ is the corrected bottom hole temperature, T_s is the surface temperature, and Z is the depth. The surface temperature was estimated on the basis of correlation with elevation.
5. **Interpolation and Map Creation:** A minimum curvature interpolation method was used with specific parameters in the Geosoft software. The map was edited in ArcMap, including official coverages of sedimentary basins and coverage of points with conventions for differentiating the magnitude of the estimated gradient and the measured BHT depth.

The geothermal gradient values are predominantly ranging between 10 and 40 °C/Km, as shown in Figure 4b. The data exhibit a unimodal distribution, characterized by a pronounced peak and a right-skewed asymmetry, indicating a longer tail of higher geothermal gradient values.

The distribution suggests that we are working with an imbalanced dataset, while the majority of measurements are clustered at lower gradients, a subset of regions exhibits elevated gradients, potentially highlighting areas of heightened geothermal activity. This skewness towards higher values contributes to an increased error rate in the model when predicting in these less represented higher gradient zones.

To deal with underrepresented high-gradient values, we defined a frequency-based weighting so that the less-frequent gradients within a 15-bin histogram distribution have the higher weights, and the most-frequent gradients have the lowest weight (Figure 5). The number of bins and, therefore, the values of the weights; were adjusted based on model evaluation.

Furthermore, it is important to consider that the geothermal gradient data have an inherent bias: Although the measurements were made mainly in basins, a considerable amount of the data is close to Andean and volcanic areas, so measurements made in areas farther away tend to be underrepresented and affected the prediction for areas where there are no measurements. To correct for this bias, we defined each high-gradient well located more than 75 km from the nearest volcano as "non-volcanic" and assigned a weight of 8 to those wells.

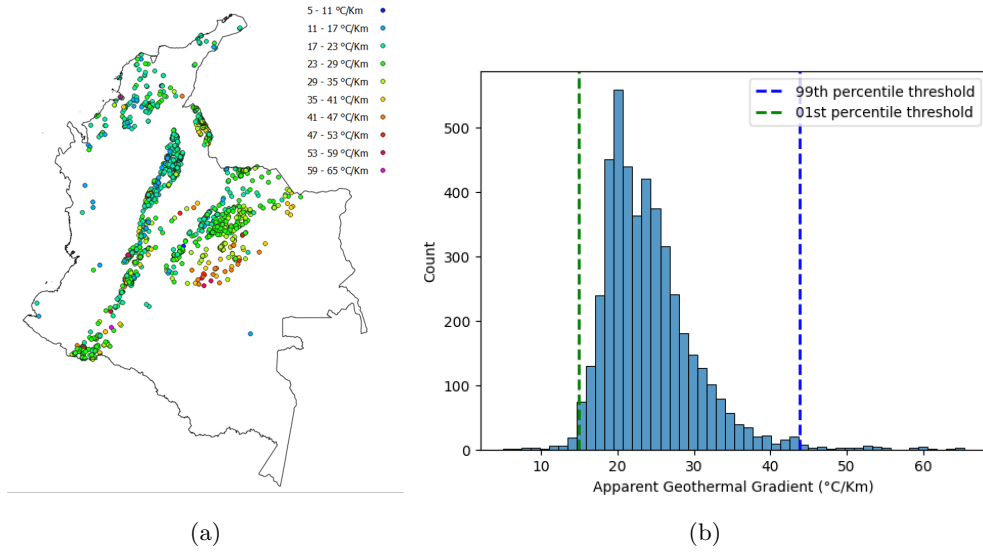


Fig. 4: (a) Measured geothermal gradients in Colombia, (b) Histogram of apparent geothermal gradient values indicating a right-skewed distribution. Dashed lines indicated the representative percentiles for lowest and extreme gradients that will be discarded.

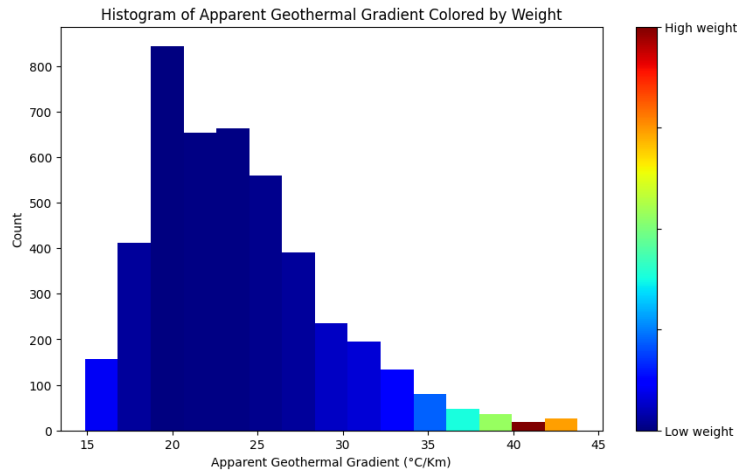


Fig. 5: 15-bin frequency histogram showing the weighting distribution for the geothermal gradients. The weights were normalized so the highest weight is 1.0 and the lowest is 0.02.

Finally, we constrained the training and test sets to a specific range: from the 1st percentile value of 14.87 °C/km to the 99th percentile value of 43.80 °C/km (Figure 4b). This selection ensures that the model is trained and evaluated in a confidence range.

5.2 Geological and Geophysical Data

To predict the apparent geothermal gradient, we utilized a diverse array of geological and geophysical data. This data provided insight into the subsurface conditions necessary for accurate geothermal gradient estimation.

The AGG dataset includes latitude and longitude, for georeferencing well sites. This geospatial positioning is used to integrate the spatial variations of the geothermal data into the model. Alongside these coordinates, topography and elevation play a significant role. The topographic elevation data, derived from well data and NASA’s global Earth Digital Elevation Model (DEM) as of 2021, provide a vertical reference point which is essential for geothermal gradient measurements.

Additionally, subsurface characteristics are another key aspect of the dataset. Insights into the thermal structure of the lithosphere and the behavior of heat at depth are garnered from the depths to the Moho discontinuity and the Curie isotherm. These are sourced from studies by Quintero et al. (2014) and Uieda & Barbosa (2017). Moho discontinuity and elevation data are strictly correlated to lithosphere thickness, which is a great predictor for the geothermal gradient in the continent (Kolawole & Evenick, 2023); Studies from Quintero et al (2019) and Ponce & Hernández (2014) show that there is an inverse correlation between the thermal gradient and the Curie isotherm. The depth of lithosphere-asthenosphere boundary was regarded as one of the top five important features in previous models (e.g., Rezvanbehbahani et al., 2017; Lösing and Ebbing, 2021), however, it was discarded because of the lack of a representative dataset for Colombia.

Additionally, the presence of geophysical anomalies significantly influences the dataset. Magnetic anomalies, documented in the WDMAM V2 map by Dymant et al. (2020), are important as they potentially correlate with AGG. The deepest magnetic sources can be associated to the Curie depth (Lösing & Ebbing, 2021).

Gravity anomalies are also strong indicators of crustal composition. We use Free Air anomalies and Vertical Gravity Gradients from Sandwell et al. (2021) and Pavlis et al. (2012) datasets, it can indicate variations in the subsurface composition and structure. These variations are essential in understanding the distribution of subsurface heat and are influenced by crustal properties, such as the density variations and their correlation with rock types. The Bouguer anomaly was calculated using the Free Air anomaly with the Bouguer correction, and using this parameter allows us to reduce the elevation influence in the gravitational anomaly. After testing, we decided to keep the three gravity features.

The dataset also considers fault data, specifically the proximity to faults, calculated using data from Gómez et al. (2020) and analyzed through a Nearest Neighbors Algorithm. This proximity provides insights in evaluating potential permeability and fluid flow, which can significantly affect subsurface thermal regimes. Active faults, in

particular, identified by Veloza et al. (2012), are of immense importance due to their potential role in localizing geothermal systems.

Lastly, the depth to the basement rocks (igneous and metamorphic) is a critical factor in understanding the influence of subsurface rock types on thermal behavior, as they are a main source of radiogenic heat production compared to sedimentary rocks (Hasterok et al., 2018). Due to the absence of a specific basement depth model, an alternative method is employed using the geological map by Gómez et al. (2015). This method involves classifying rock outcrops as either basement or non-basement (sedimentary and deposits), and measuring the distance from each well site to the nearest basement outcrop. This assessment helps to understand the impact of these rocks on geothermal gradients.

Integration of geospatial coordinates, topographical data, subsurface characteristics, geophysical anomalies, fault data, and proximity to basement rocks forms a comprehensive framework for accurately modeling and understanding the subsurface geothermal behavior, reflecting the multidisciplinary nature of geothermal research. Each of these factors contributes uniquely to understand the gradient distribution, underlining the complex interplay of geological, geophysical, and spatial factors in geothermal exploration and modeling.

Detailed descriptions of these variables are provided in Table 1 and two graphical examples are shown in figure 6. The correct interpretation and use of these data is crucial for predictive modeling of geothermal gradients across Colombia. The features were directly interpolated to obtain values at specific geographic points without resampling, the dataset with the lowest resolution (Moho Depth) has a 0.4° latitude-longitude grid.

5.3 Hyperparameter tuning

To optimize the performance of the model, we defined a grid of hyperparameters. The code iterates through these hyperparameter combinations, training the model, and evaluating mean squared error (MSE) on the test set for each configuration. The process systematically identifies the combination of hyperparameters that minimizes MSE, ensuring the model is fine-tuned for optimal predictive accuracy on the given dataset (Table 2).

6 Results

The result we present for this study is a predicted geothermal gradient map for all the Colombian territory. The accuracy of the methodology is evaluated using the test subset derived from the initial dataset partitioning. We examine the key performance metrics: MAE, RMSE, nMAE, nRMSE and the coefficient of determination (R^2) to quantify the predictive precision of the model. Additionally, we employ visualizations to facilitate a comprehensive analysis: plots for actual versus predicted values, diagrams illustrating feature importances, and assessments delineating the influence of individual features on the model’s output.

A geospatial comparison of actual data against model predictions is conducted to discern the model’s spatial prediction accuracy. This comparison not only substantiates the model’s validity, but also underscores any region-specific deviations.

Table 1: Geological and geophysical features used in the study with their respective sources.

Feature	Description	Source
Elevation (m)	Height above sea level.	NASA Visible Earth (2021)
Moho Depth (m)	Depth to the Mohorovičić discontinuity.	Uieda & Barbosa (2017)
Curie Depth (Km)	Depth at which rocks in a specific geographical area encounter the Curie temperature	Quintero et al. (2014)
Magnetic Anomaly (nT)	Earth’s magnetic field anomaly at the point.	Dyment et al. (2020)
Free Air Anomaly (mGal)	Gravity anomaly after Free Air correction	Sandwell et al. (2021)
Bouguer Anomaly (mGal)	Gravity anomaly after Free Air correction and Bouguer corrections	Sandwell et al. (2021)
Vertical Gravity Gradient (E)	rate of change of vertical gravity (gz) with height (z)	Pavlis et al. (2012)
Faults (m)	Distance to the nearest normal, reverse or strike-slip fault.	Gómez et al., (2020)
Active Faults (m)	Distance to the nearest active fault.	Veloza et al., (2012)
Distance to basement (m)	Surface distance to igneous or metamorphic outcrops	Gómez et al., (2015)
Volcanic Domain	Boolean variable to define whether the well is located in a volcanic zone or not.	Gómez et al., (2020)
AGG measurements (°C/Km)	Target variable, measured from bottom hole data	Alfaro et al., (2009)

Table 2: Best Hyperparameters after Model Tuning

Hyperparameter	Value	Meaning
max_depth	10	Maximum depth of a tree.
learning_rate	0.1	Step size shrinkage used in updates.
gamma	0.0	Minimum loss reduction required to make a further partition.
min_child_weight	1	Minimum sum of instance weight needed in a child.
colsample_bytree	0.5	Fraction of features to be randomly sampled for each tree.
reg_alpha	0.5	L1 regularization term.
reg_lambda	0.5	L2 regularization term.
subsample	1	Fraction of training data to be randomly sampled for each boosting round.

6.1 Model Validation

The initial phase of the model evaluation involved scrutinizing its performance in both the training and the test subsets, the latter representing previously unseen data. For the training set, the model achieved an MAE of 1.4793, an RMSE of 2.1371, and a coefficient of determination (R^2) of 0.8287. These metrics are typical for models evaluated on their training data. Conversely, the test data got an MAE of 2.6826, an RMSE of 3.5842, and an R^2 of 0.5497.

The disparity in R^2 could be attributed to several factors, including the under-representation of higher geothermal gradient values, the geographic bias of the measurements and the inherently complex nature of the dataset. The test set’s normalized error metrics, nMAE and nRMSE, were recorded at 0.06 and 0.12 respectively,

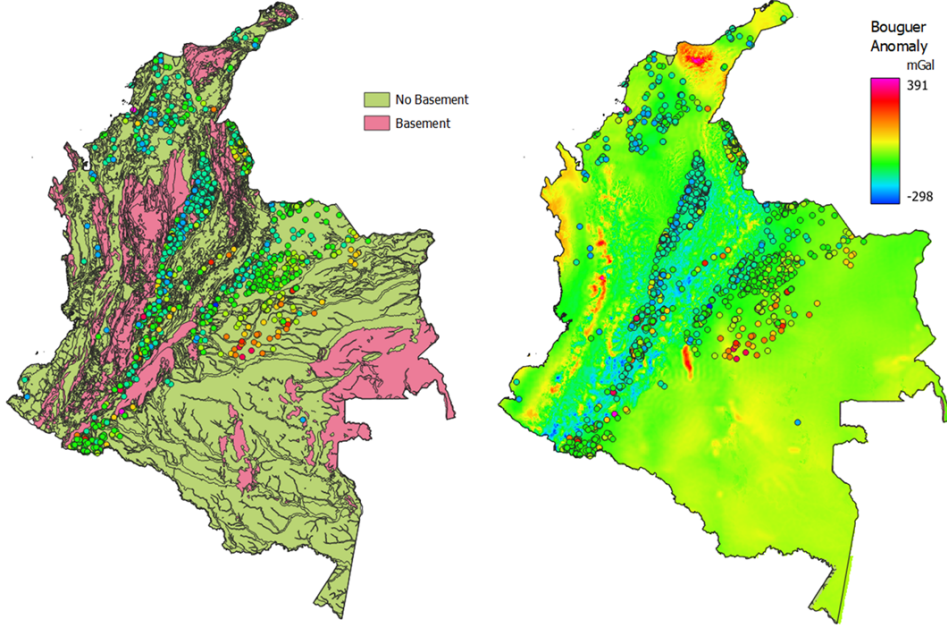


Fig. 6: Side-by-side maps of Basement rocks outcrops and Bouguer anomaly with the measured gradient locations.

indicating that our predictions are expected to be within a range from 6% to 12% of the correct values.

A detailed examination of the residuals, as depicted in Figure 7, reveals a random distribution around the zero line. This pattern suggests an absence of bias in the residuals, corroborated by a residual mean close to zero, indicating that the model is on average neither overestimating nor underestimating significantly. However, points with high residuals highlight instances where model performance was suboptimal, though most residuals cluster near zero.

Regarding the plot of actual versus predicted values, illustrated in Figure 8, the concentration of points along the ideal prediction line indicates proficient modeling of the target values. The dispersion of points as the target value increases suggests increasing variance in the model's predictions. The model demonstrates higher accuracy for lower actual values while tending to underestimate higher actual values in the test set. The overlap of training (blue) and test (red) data points in the plot is indicative of good model generalization, evidenced by the similarity in performance across the training and test datasets. This overlap is a positive sign, suggesting that the model is not overfitting to the training data and most of the variance in the test set is towards the high gradient values.

Evaluating the model's geospatial predictive performance is crucial for understanding its applicability in practical scenarios. This involves a comparative analysis of observed geothermal gradient values against the model's predictions.

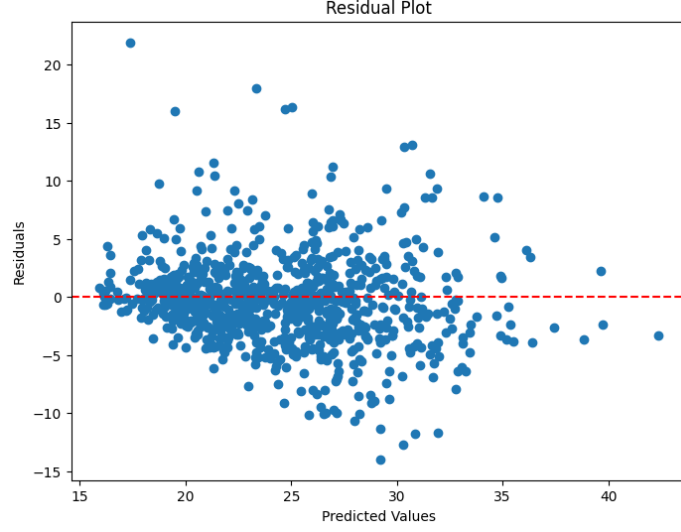


Fig. 7: Residuals distribution of the model.

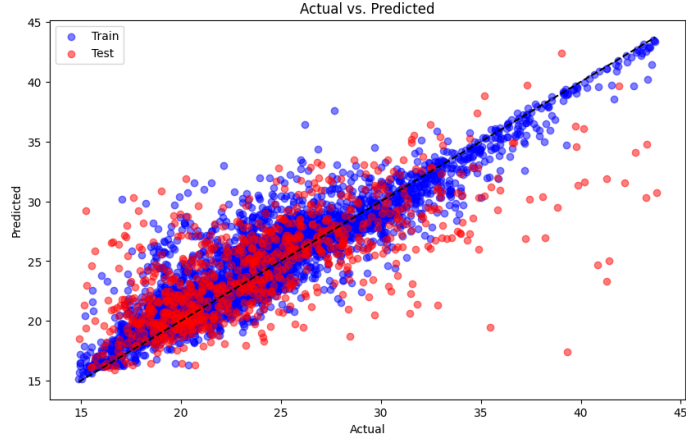


Fig. 8: Actual vs. Predicted values plot comparing the training and test subsets.

Additionally, a side-by-side visualization of the actual and predicted geothermal gradient values was carried out, as shown in Figure 9. The actual values map is a representation of empirically measured geothermal gradients used for the training , while the predicted values map is derived from the model estimations. The consistency of geothermal gradients across both maps serves as an indicator of the model's spatial accuracy.

The Figure 10 highlights the differences between the actual and the predicted geothermal gradient values, showing regions where the model's predictions deviate

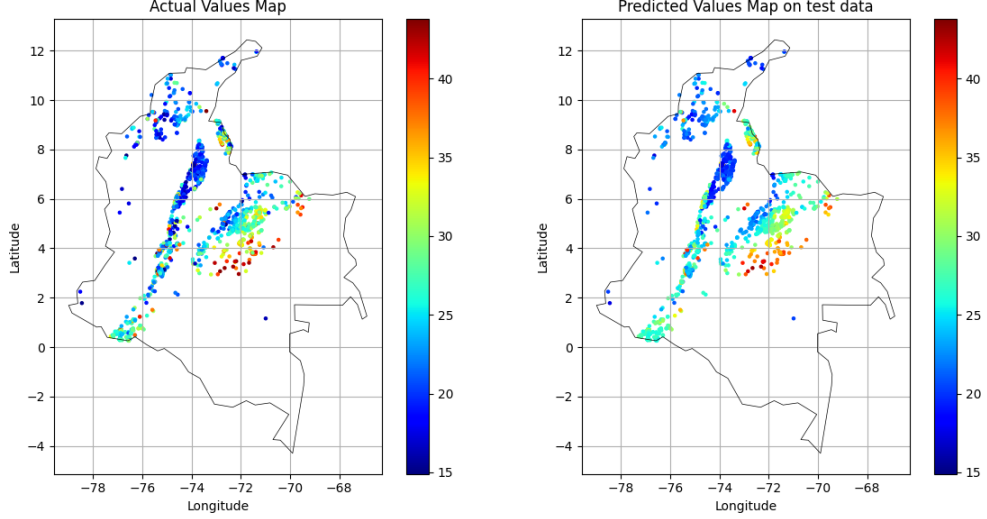


Fig. 9: Side-by-side comparison of actual and model-predicted geothermal gradient values, highlighting the model's spatial prediction accuracy.

from measured data. Those discrepancies suggest potential areas for model enhancement or may pinpoint inherent limitations within the data or the model's structural assumptions. The tendency of the model to underestimate geothermal gradients, specially when they are higher, indicates possible gaps in its representation of heat source distribution or heat transfer mechanisms, and may require data enhancement.

Comparing actual with predicted values yields critical insights into the model's predictive strengths and weaknesses. Such an assessment is imperative to refine the model's predictive capabilities, thereby enhancing its contribution to geothermal exploration and resource evaluation.

6.2 Feature importance analysis

Feature importance provide insight into which variables are most informative for making accurate predictions. Multiple techniques were used to determine the importance of the features, each offering a unique perspective on the data.

Weight-Based Importance

The weight-based feature importance, as shown in Figure 11, indicates that active faults, elevation and Moho depth are the most frequently used features in the model to make decisions, with structural features and basement proximity having also a high importance. Potential fields and Curie Depth, on the other hand, are less frequently used. The importance is equilibrated among most of the features. This highlights the model's reliance on all the data to predict the target variable, especially topography, subsurface discontinuities, and structural influence.

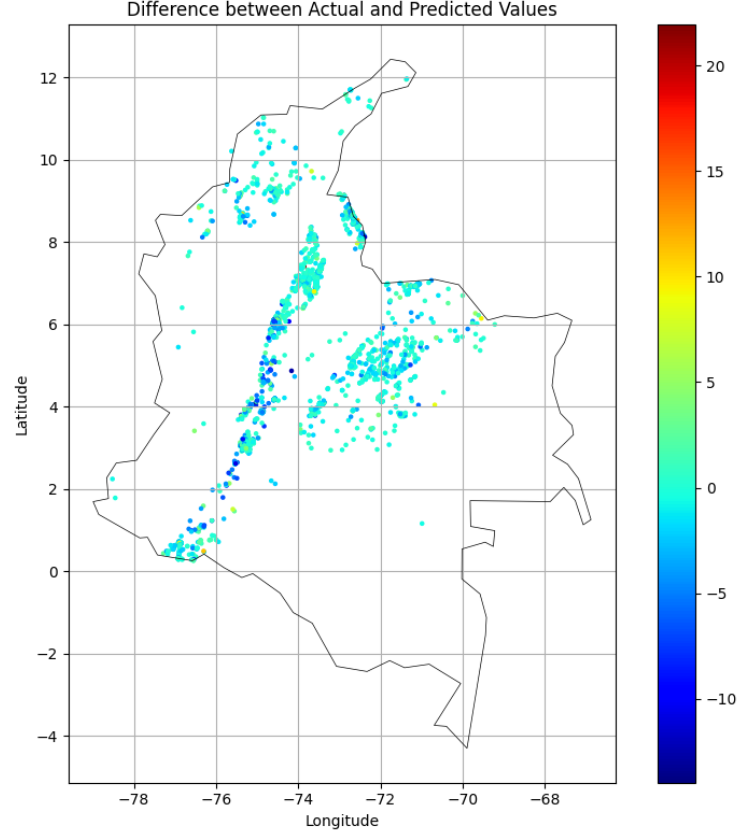


Fig. 10: Differences between actual and model-predicted geothermal gradient values.

Gain-Based Importance

Figure 12 presents the gain-based feature importance, which reflects the improvement in accuracy brought by a feature to the branches, how the features contributed to minimize the loss function, and, subsequently, to the model's performance. Basement proximity in surface emerges as the most significant predictor, and features such as Potential fields and Curie Depth play a significant role here as well; however, most of the features importances are equilibrated.

Mutual Information

Mutual information scores, as shown in Figure 13, quantify the dependency between each feature and the target variable. Moho depth is seen to be highly informative, along with the geophysical and structural data.

We also evaluated each individual feature using the model score, the R2 score, the normalized root mean square error (nRMSE), and the normalized mean absolute error (nMAE). As shown in Figure 14, each metric is visualized for every feature after training the model with each individually.

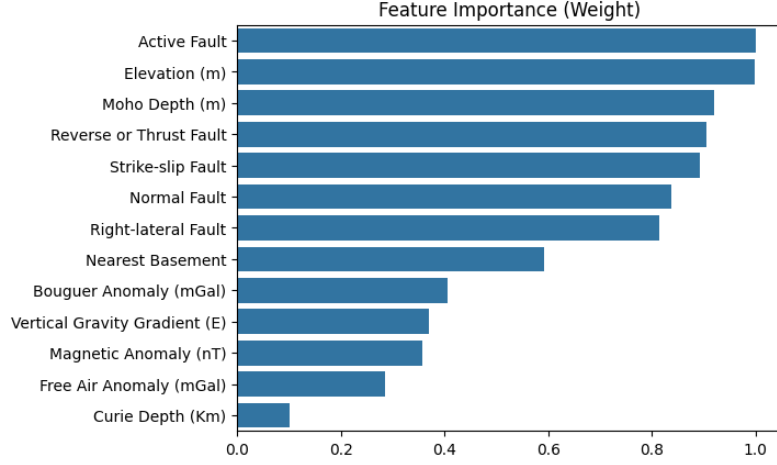


Fig. 11: Weight-based feature importance plot.

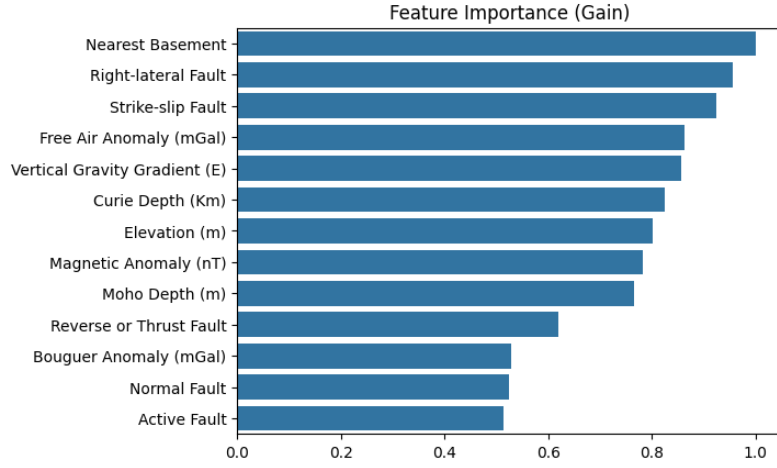


Fig. 12: Gain-based feature importance plot.

Moho depth and geophysical measurements, such as the Free Air Anomaly, consistently demonstrated high importance as isolated predictors. In contrast, the topography and Curie depth showed lower individual relevance.

Assessing the model's performance as a function of the feature count, starting with the less important (gain-based) and so on, reveals an increase in both the model score for the training set and the R^2 score for the test set, as shown in Figure 15. These increments signify enhanced precision and variance explanation. Nonetheless, the progressive improvement in scores flatten after incorporating roughly nine features, indicating that further features may not substantially enhance the model's error metrics. It is essential to note, however, that each feature significantly enhances the

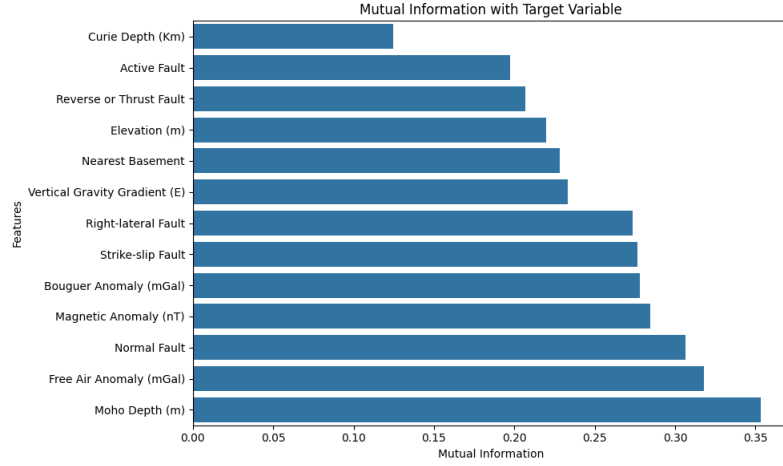


Fig. 13: Mutual Information with the target variable.

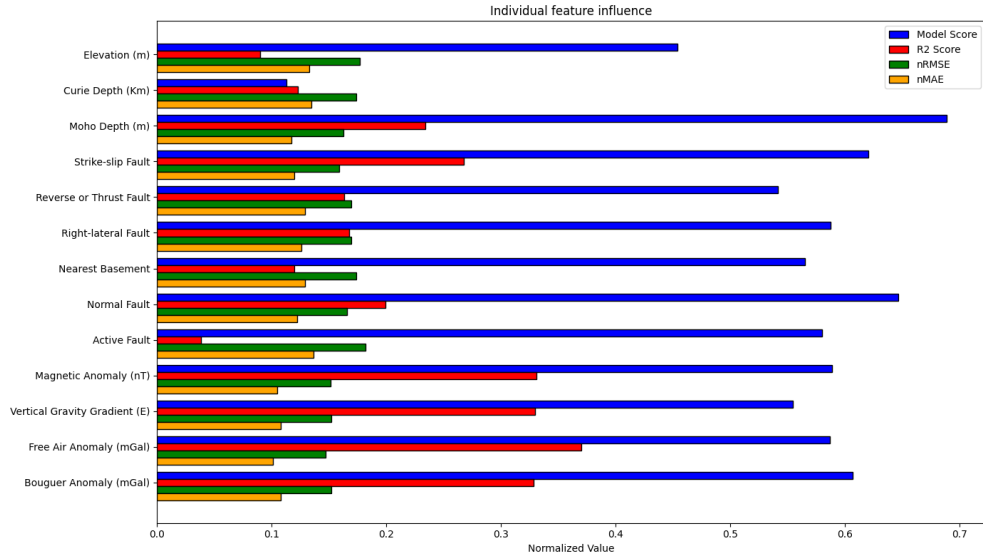


Fig. 14: Feature importance evaluated by various metrics for each individual feature. Values are normalized.

model's spatial precision, as suggested by the feature importance and mutual information data. Thus, excluding any feature could negatively affect the outcomes: while performance levels off after nine features, the remaining features should not necessarily be dismissed. Incorporation of particularly insightful features, like the actual depth to the basement, depth of lithosphere-asthenosphere boundary or improved feature resolution could, indeed, offer advancements to the model.

The analyses suggest that a subset of features provides the most predictive power without introducing unnecessary complexity or risking overfitting. This balance is crucial for developing a model that is both accurate and generalizable.

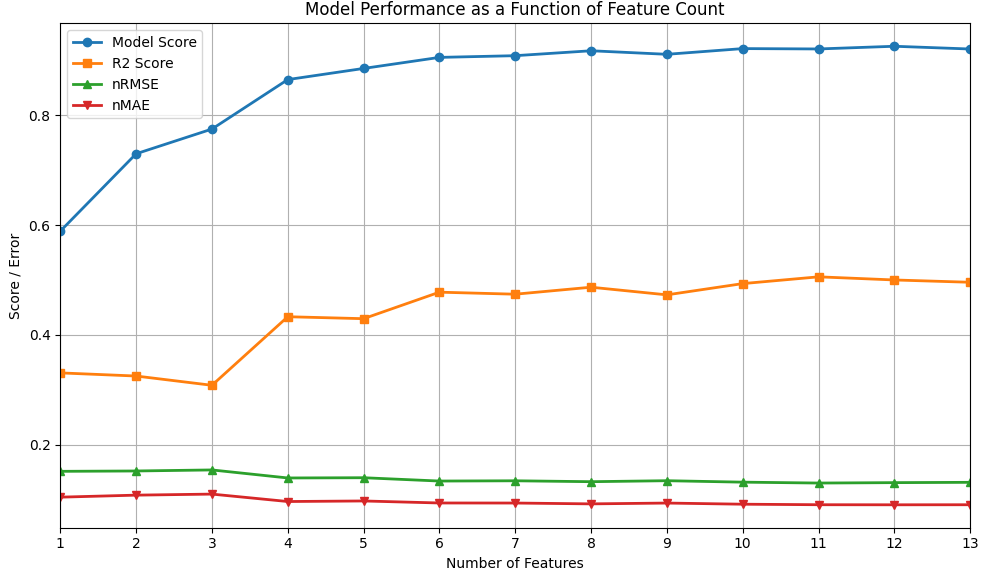


Fig. 15: Model performance as a function of the number of features included, starting from the less important (gain-based).

6.3 Spatial Distribution of Predicted Geothermal Gradients

The spatial distribution of the predicted geothermal gradients is a key factor in evaluating the utility of the model for geothermal exploration. Figure 16 illustrates the geothermal gradients predicted in the study area. The color gradient from blue to red indicates increasing values, and warmer colors represent a higher geothermal potential.

The map offers practical information on areas with significant geothermal activity, marking them as prime candidates for detailed exploration and potential development; however, it's important to understand the model limitations and, therefore, the fact that some high-gradient zones tend to be underrepresented. The effectiveness of the predictive model lies in its ability to identify these spatial variations and key trends, this characteristic making it a valuable asset in the guide of exploration strategies toward the most promising geothermal energy locations.

7 Discussion

The evaluation of our predictive model for the estimation of geothermal gradients has been extensive, incorporating a variety of metrics and visual analyses. Training set

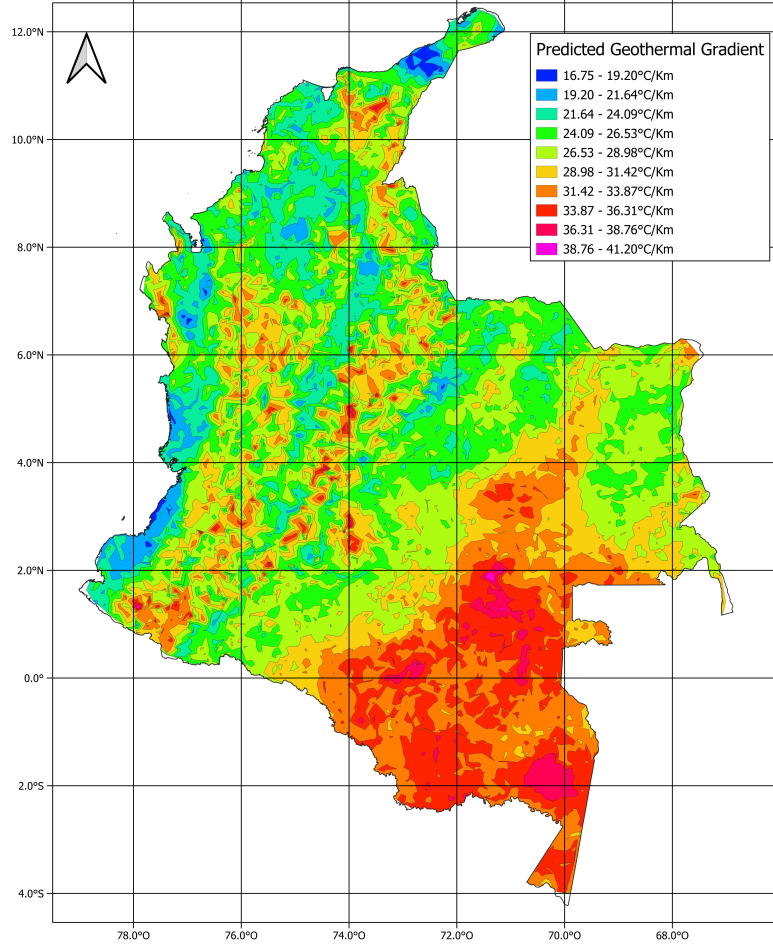


Fig. 16: Predicted geothermal gradient map showing the spatial distribution of geothermal potential across the region.

metrics, MAE, RMSE, and R-squared, along with the corresponding test set metrics provide a comprehensive view of the model performance. The model shows strong performance in the training set, with an MAE of 1.47, an RMSE of 2.14, and an R-squared value of 0.83, as indicated in Section 6.1. These values reflect a high degree of accuracy and a strong correlation between the predicted and actual geothermal gradients, suggesting that the model is capable of capturing the underlying patterns within the training data. However, when applied to the test set, the model's performance drops, with an MAE of 2.68, an RMSE of 3.58, and an R-squared value of 0.55, as detailed in Section 6.1. The observed increase in error and the decrease in the R^2 value on the test set, as opposed to the training set, may suggest possible overfitting, particularly in the context of estimating higher values of geothermal gradients where the data are

less abundant. Despite this, the model’s ability to generalize is demonstrated to be effective, as illustrated in Figure 8.

Comparative analysis with related studies highlights the effectiveness of our model. For example, the study by Lösing & Ebbing (2021) in Antarctica achieved an nRMSE of 0.29 and an R^2 of 0.45, while Rezvanbehbahani et al. (2017) in Greenland recorded an nRMSE of 0.15 and an R^2 of 0.6. Our results, with an nRMSE of 0.12 and an R^2 of 0.55, reflect not only a lower relative error compared to these studies, but also a balanced performance in terms of the determination coefficient. This comparison highlights the accuracy and reliability of our model in different geological settings.

Our feature importance analyses, comprising weight-based, gain-based, and mutual information methods, showcased the varying impact of different features. Elevation and proximity to the basement consistently emerged as the main predictors of multiple importance measures, as discussed in Sections 6.2. Moho depth is also one of the most important predictors, and its relation with the lithospheric thickness suggests an agreement with the correlation of this tectonic feature with the thermal gradient defined by Kolawole & Evenick (2023). The geophysical properties, such as Bouguer or Free Air Anomaly, have been highlighted as significant by certain importance methods but appear less influential in others.

The observed discrepancies between training and test performance may indicate the need for further model refinement or data enhancement. Strategies such as feature engineering, parameter optimization, and integration of more specific data such as actual depth to basement or lithosphere thickness could be employed to enhance the model’s predictive power and generalizability.

The geospatial distribution of the predicted geothermal gradients, illustrated in Figure 16, highlights the spatial prediction capabilities of the model. The alignment of high-gradient regions on actual versus predicted maps (Figure 10) and the regions of significant discrepancy provide a nuanced understanding of the spatial precision of the model.

The model’s output indicates a distinct sensitivity to geothermal indicators, revealing high-gradient values that are suggestive of underlying geothermal resources. These values are particularly pronounced in regions characterized by volcanic activity or where the crust is considerably thinner. A standout feature of the model is its predictive accuracy in the Amazon basin (Colombian portion is called Vaupés-Amazonas Basin, as per Figure 2b), where data scarcity has previously been a barrier. The gradient predictions of the model for this area not only fill a critical data gap, but also exhibit remarkable agreement with the findings from the Pimentel & Hamza (2012) study of the Brazil’s portion of the basin (Figure 17). This concordance is a testament to the model’s robustness and its ability to extrapolate from known data to regions lacking in situ measurements.

While the predicted map tends to underestimate high gradients, as seen in previous sections, we can infer that the geothermal gradient model is effectively capturing areas with geothermal potential, especially where geological structures such as faults are prevalent, and thermal manifestations are observed (refer to Figures 3 and 2a). This suggests that the geothermal model could serve as a valuable tool for targeting exploration efforts. Furthermore, the correlation between high-gradient areas and

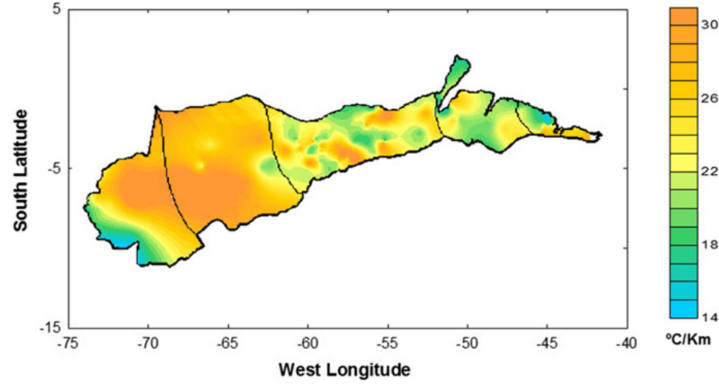


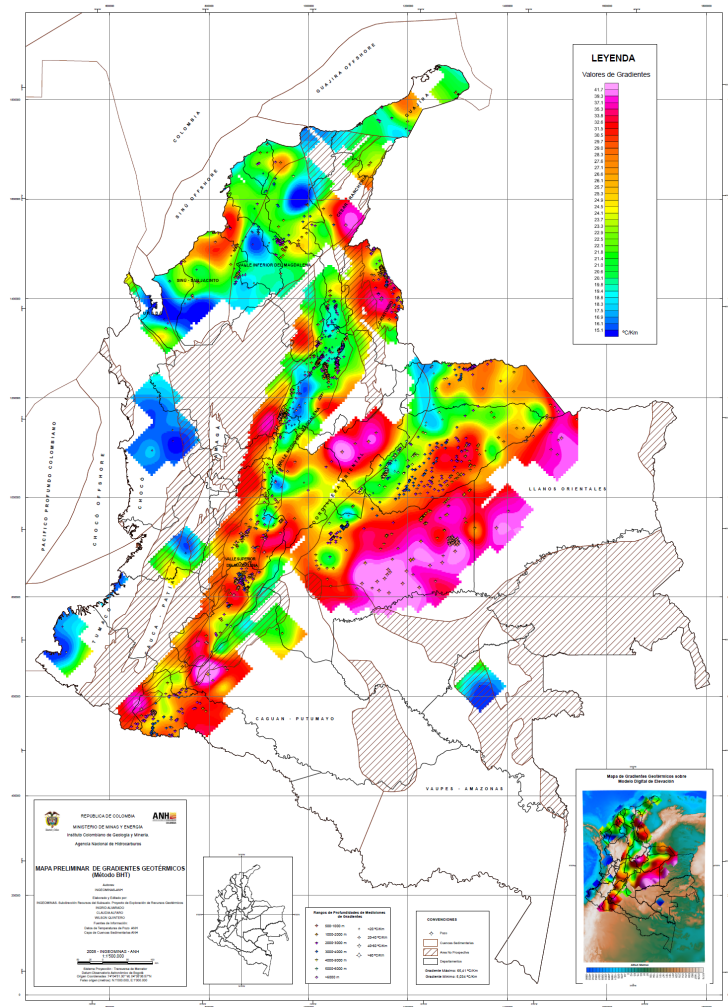
Fig. 17: Geothermal gradient of the Amazon Basin at the north-west Brazil, showing a predominantly trend of high-gradient values. Taken from Pimentel & Hamza (2012)

volcanic activities, as well as fault distributions and basement (igneous and metamorphic) rocks, could inform a more detailed geothermal potential map that includes both predicted gradients and direct geological measurements.

Comparison between our predicted map and the preliminary geothermal gradient map (Figure 18) shows that while the predicted map provides a competent representation of geothermal trends (as discussed previously), underestimating high gradients leads to significant differences in certain areas, such as the west of Eastern-Llanos and Caguán-Putumayo basins (see Figure 2b). This trend towards underestimation is likely attributed to an under-representation of higher gradient data in the training dataset. While we have attempted to mitigate this issue by assigning greater weights to these less frequent, high gradient instances (Figure 5), it is evident that acquiring and integrating additional high-gradient data is essential for enhancing the model's accuracy in these critical areas. Further refinement in data collection and integration techniques will be crucial to improve the representation of high geothermal gradients by the predictive model.

Our predicted geothermal gradient map, when compared with more contemporary and methodologically varied maps such as the one produced by Gómez et al. (2019) for northwestern Colombia (a region characterized by data scarcity), which was calculated through seismic interpretation and phase diagram analysis to determine temperature and pressure differences (Figure 19a), presents some discrepancies, particularly in very-low gradient values. These discrepancies could be attributed to the potential under-representation of low gradient values in our dataset, as well as to the general paucity of data in the region, as illustrated in Figure 4a. The methodology followed by Gómez et al. (2019) might also contribute to the observed variances between their findings and the predictions of our model.

Conversely, when comparing our predicted geothermal gradient map with the one developed by Matiz-León (2023) for the Eastern-Llanos (Figure 19b), which utilized a geo-statistical methodology, there is a notable congruence in gradient distribution. It's important to mention, however, that Matiz-León's map indicates somewhat higher



gradient values. This discrepancy may arise from a variety of factors, including the different methods applied (geo-statistical modeling and interpolation over a localized area versus our machine learning approach applied countrywide) as well as under-representation of high gradient data for training our model.

It is also crucial to acknowledge the variations observed between the maps of Matiz-León (2023) and Gómez et al. (2019) when compared to the preliminary geothermal gradient map by Alfaro et al. (2009). Such differences not only underscore the intrinsic challenges of estimating geothermal gradients in Colombia but also how different methodological frameworks can yield slightly different results. These discrepancies

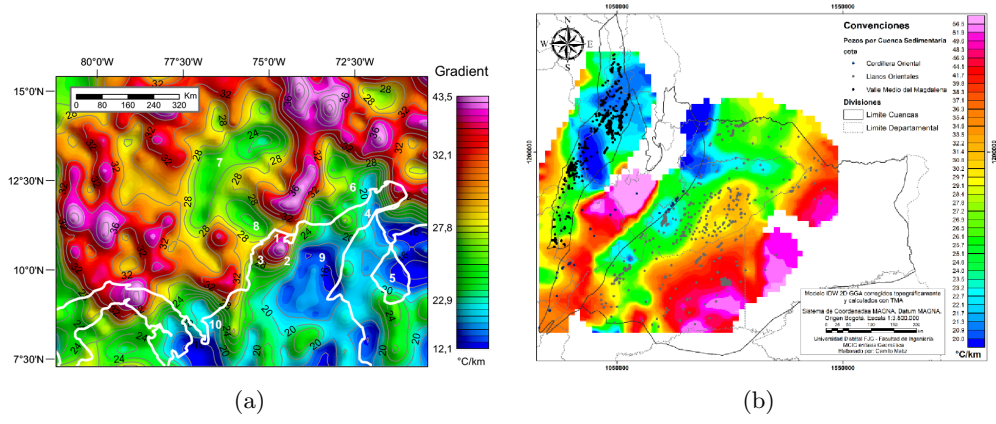


Fig. 19: (a) Colombian-Caribbean Geothermal Gradient Map. White line indicates the littoral and border lines of Colombia Venezuela and Panama. Taken from Gómez et al. (2019). (b) Geothermal gradients for Eastern-Llanos basin. Taken from Matiz-León (2023).

could potentially be mitigated by enriching the dataset with more direct measurements, particularly in regions that are currently data-deficient. This would enable a more refined and accurate estimation of the country’s geothermal gradient landscape.

In terms of new discoveries, the model highlights areas with potentially high geothermal gradients that are not documented in existing gradient maps. These predicted hotspots, particularly in the uncharted Amazon region, present opportunities for exploration and possible development of geothermal resources. The model has proven to be a valuable asset in geothermal exploration, especially for the Amazon of Colombia, where it predicts high geothermal gradients in the absence of empirical data. Its alignment with the established geothermal gradients from Pimentel & Hamza’s work, and its similarity to other gradient maps, further validates its predictive capacity.

Indeed, the application of data-driven methods like Machine Learning in predicting geothermal gradients is inherently reliant on the quantity and quality of available field data. This reliance emphasizes an ongoing opportunity for enhancement, as additional data can be used to continuously refine the model. Such improvements are expected to significantly enhance the model’s utility in the precise identification and assessment of geothermal resources. As the model continues to be refined, its role in the identification and assessment of geothermal resources is expected to become critical, supporting a more informed and strategic approach to energy exploration in the region.

The spatial distribution of the predicted geothermal gradients provide critical guidance for geothermal exploration. These tools enable the strategic prioritization of regions for further investigation, allowing for a focused allocation of resources to areas with the highest geothermal potential. The regions with the highest predicted gradients warrant immediate attention for exploration and data acquisition. These areas, flagged by the model, are likely candidates for sustainable geothermal development.

In contrast, areas with lower predicted gradients can be investigated for baseline data collection, contributing to a more comprehensive understanding of the geothermal profile of the region.

Our predictive model can play a pivotal role in the early stages of exploration, for example, inform decision-making processes regarding site selection for geothermal power plants and drilling operations. By leveraging the model’s predictions, stakeholders can enhance their exploration strategies, targeting locations with a higher likelihood of geothermal activity, and thereby advancing the exploration for renewable energy sources. This optimized approach promises not only greater efficiency in resource utilization but also a higher success rate in developing geothermal energy projects.

8 Conclusion

This study has successfully developed a machine learning model to estimate geothermal gradients across Colombia, marking a significant contribution in the field of geothermal energy exploration. By utilizing diverse geophysical and geological data, and gradient boosting regression; we have created a model that displays accurate gradient predictions across unexplored regions in Colombia.

Our model illustrates the potential of machine learning in enhancing the understanding of geothermal gradients distribution, specially within the context of Colombia, where there are vast regions whose geothermal energy has been underexplored (or not explored at all) due to the lack of extensive well data.

The incorporation of a wide range of geological and geophysical features was crucial to our approach, which allowed for a better understanding of the factors influencing geothermal gradients and heat distribution within the subsurface. The findings of this study mark a substantial step forward in geothermal exploration efforts, providing a promising tool for the identification of regions with significant geothermal potential. This advancement is expected to greatly assist in the prioritization of future geothermal exploration plans, making it a valuable asset for both researchers and industry professionals.

As we look to the future, the study encourages further research to refine and enhance the model’s accuracy. This includes the integration of local or regional data instead of global data, and the exploration of additional features that may influence geothermal gradients. Finally, we highlight the capability of machine learning to contribute, through continued improvements, to the sustainable development of Colombia’s geothermal resources and other renewable energy sources.

9 Data Availability

The data supporting the findings of this study are openly available in the GitHub repository associated with this project. Interested parties can access the dataset, additional resources, and the code used for the analyses at the following URL:

<https://github.com/jcmefra/Geothermal-Gradient-Machine-Learning>

This repository includes all relevant data, scripts, and additional materials required to replicate the study’s results or to further explore the geothermal gradient estimation

model. By providing the data in a public domain, we encourage transparency, reproducibility, and collaborative efforts to enhance the research in geothermal gradient prediction using machine learning techniques.

References

- [1] Afonso, J. C., Salajegheh, F., Szwillus, W., Ebbing, J., & Gaina, C. (2019). *A global reference model of the lithosphere and upper mantle from joint inversion and analysis of multiple data sets.* Geophysical Journal International, 217(3), 1602-1628. <https://doi.org/10.1093/gji/ggz094>
- [2] Alfaro, E., Vargas, C. A., & Gutiérrez, J. (2009). *Mapa preliminar de gradientes geotérmicos de Colombia.* Servicio Geológico Colombiano. <https://catalogo.sgc.gov.co/cgi-bin/koha/opac-detail.pl?biblionumber=49454>
- [3] Alfaro, C., Rueda-Gutiérrez, J. B., Casallas, Y., Rodríguez, G., & Malo, J. (2021). *Approach to the geothermal potential of Colombia.* Geothermics, 96, 102169. <https://doi.org/10.1016/j.geothermics.2021.10216>
- [4] Alqahtani, F., Ehsan, M., Abdulfarraj, M., Aboud, E., Naseer, Z., El-Masry, N. N., & Abdelwahed, M. F. (2023). *Machine learning techniques in predicting bottom hole temperature and remote sensing for assessment of geothermal potential in the Kingdom of Saudi Arabia.* Sustainability, 15(17), 12718. <https://doi.org/10.3390/su151712718>
- [5] Assouline, D., Mohajeri, N., Gudmundsson, A., & Scartezzini, J. L. (2019) *A machine learning approach for mapping the very shallow theoretical geothermal potential.* Geothermal Energy, 7(1), 1-50. <https://doi.org/10.1186/s40517-019-0135-6>
- [6] Bachu, S., Ramon, J. C., Villegas, M. E., & Underschultz, J. R. (1995). *Geothermal regime and thermal history of the Llanos Basin, Colombia.* AAPG bulletin, 79(1), 116-128. <https://doi.org/10.1306/8D2B14D0-171E-11D7-8645000102C1865D>
- [7] Békési, E., Struijk, M., Bonté, D., Veldkamp, H., Limberger, J., Fokker, P. A., Vrijlandt, M., & van Wees, J.-D. (2020). *An updated geothermal model of the Dutch subsurface based on inversion of temperature data.* Geothermics, 88, 101880. <https://doi.org/10.1016/j.geothermics.2020.101880>
- [8] Burton-Johnson, A., Dziadek, R., & Martin, C. (2020). *Geothermal heat flow in Antarctica: Current and future directions.* The Cryosphere Discussions, 1–45. <https://doi.org/10.5194/tc-14-3843-2020>
- [9] Chen, T., & Guestrin, C. (2016). *Xgboost: A scalable tree boosting system.* In Proceedings of the 22nd ACM SIGKDD International Conference on Knowledge Discovery and Data Mining (pp. 785-794). <https://doi.org/10.1145/2939672.2939785>

- [10] Clavijo, J., Mantilla, L., Pinto, J., Bernal, L., Pérez, A. (2008). *EVOLUCIÓN GEOLÓGICA DE LA SERRANÍA DE SAN LUCAS, NORTE DEL VALLE MEDIO DEL MAGDALENA Y NOROESTE DE LA CORDILLERA ORIENTAL*. *Boletín de Geología*, 30(1), 45-62.
- [11] Dyment, J., Choi, Y., Lesur, V., Garcia-Reyes, A., Catalan, M., Ishihara, T., Litvinova, T. & Hamoudi, M. (2020, May). *The World Digital Magnetic Anomaly Map: version 2.1*. In EGU General Assembly Conference Abstracts (p. 22098). <https://doi.org/10.5194/egusphere-egu2020-22098>
- [12] Friedman, J. H. (2001). *Greedy function approximation: a gradient boosting machine*. *Annals of statistics*, 1189-1232. <https://doi.org/10.1214/aos/1013203451>
- [13] Gómez, J., Montes, N.E., Nivia, A. & Diederix, H. (2015). *Mapa geológico de Colombia. Escala, 1:1.000.000*. <https://datos.sgc.gov.co/maps/c05c6dbf27f645eb883bae3a9cd0d08f>
- [14] Gómez-Tapias, J., Núñez-Tello, A., Mateus-Zabala, D., Alcárcel-Gutiérrez, F. A., Lasso-Muñoz, R. M., Marín-Rincón, E., Marroquín, M. & Zabala, M. (2020). *Physiographic and geological setting of the Colombian territory.. The Geology of Colombia*, 1, 1-6. <https://doi.org/10.32685/pub.esp.35.2019.01>
- [15] Goutorbe, B., Poort, J., Lucazeau, F., & Raillard, S. (2011). *Global heat flow trends resolved from multiple geological and geophysical proxies*. *Geophysical Journal International*, 187(3), 1405-1419. <https://doi.org/10.1111/j.1365-246X.2011.05228.x>
- [16] Hasterok, D., Gard, M., & Webb, J. (2018). *On the radiogenic heat production of metamorphic, igneous and sedimentary rocks*. *Geoscience Frontiers*, 9(6), 1777-1794. <https://doi.org/10.1016/j.gsf.2017.10.012>
- [17] Kolawole, F., & Evenick, J. C. (2023). *Global distribution of geothermal gradients in sedimentary basins*. *Geoscience Frontiers*, 14(6), 101685. <https://doi.org/10.1016/j.gsf.2023.101685>
- [18] Lobo, A. (1987). *La geología de Colombia.. INGEOMINAS*, 8p.
- [19] Lösing, M., & Ebbing, J. (2021). *Predicting geothermal heat flow in Antarctica with a machine learning approach*. *Journal of Geophysical Research: Solid Earth*, 126(6), e2020JB021499. <https://doi.org/10.1029/2020JB021499>
- [20] Lucazeau, F. (2019). *Analysis and mapping of an updated terrestrial heat flow data set*. *Geochemistry, Geophysics, Geosystems*, 20(8), 4001-4024. <https://doi.org/10.1029/2019GC008389>
- [21] Marzolf, N. C. (2014). *Emprendimiento de la Energía Geotérmica en Colombia*. Felipe Herrera Library of the Inter-American Development Bank, 86.

- [22] Matiz-León, J. C. (2023). *Spatial Prediction for Bottom Hole Temperature and Geothermal Gradient in Colombia*. In Proceedings of the 48th Workshop on Geothermal Reservoir Engineering, Stanford University, Stanford, California, February 6-8, 2023 (SGP-TR-224). <https://pangea.stanford.edu/ERE/db/GeoConf/papers/SGW/2023/Matizleon.pdf>
- [23] NASA Visible Earth. (2021). *Blue Marble Next Generation w/ Topography and Bathymetry*. <https://visibleearth.nasa.gov/images/73726/june-blue-marble-next-generation-w-topography-and-bathymetry/737461>
- [24] Pavlis, N. K., Holmes, S. A., Kenyon, S. C., & Factor, J. K. (2012). *The development and evaluation of the Earth Gravitational Model 2008 (EGM2008)*. Journal of geophysical research: solid earth, 117(B4). <https://doi.org/10.1029/2011JB008916>
- [25] Pang, Y., Shi, B., Guo, X., Zhang, X., Wen, Y., Yang, G., & Sun, X. (2023). *Machine learning algorithm optimization for intelligent prediction of rock thermal conductivity: A case study from a whole-cored scientific drilling borehole*. Geothermics, 111, 102711. <https://doi.org/10.1016/j.geothermics.2023.102711>
- [26] Pimentel, E. T., & Hamza, V. M. (2012) *Indications of regional scale groundwater flows in the Amazon Basins: Inferences from results of geothermal studies*. Journal of South American Earth Sciences, 37, 214-227. <https://doi.org/10.1016/j.jsames.2012.03.007>
- [27] Ponce, P., & Hernández, O. (2014). *Estimación de la profundidad de la isoterma de Curie en parte de la zona de influencia del volcán Azufra basanda en datos geomagnéticos*. Boletín de Geología, 36(2), 79-90. <http://www.scielo.org.co/pdf/boge/v36n2/v36n2a05.pdf>
- [28] Quintero, W., Campos-Enríquez, O., & Hernández, O. (2019). *Curie point depth, thermal gradient, and heat flow in the Colombian Caribbean (northwestern South America)*. Geothermal Energy, 7(1), 1-20. <https://doi.org/10.1186/s40517-019-0132-9>
- [29] Quintero, W., Ladino, A., Lozano, E., Bolívar, O., Zamora, N., Rincón, J., & Puentes, M. (2014). *Mapa de profundidad de la isoterma de Curie para Colombia*. Servicio Geológico Colombiano. Bogotá. <https://recordcenter.sgc.gov.co/B20/23008100024725/Mapa/Pdf/2105247251300001.pdf>
- [30] Rezvanbehbahani, S., Stearns, L. A., Kadivar, A., Walker, J. D., & van der Veen, C. J. (2017). *Predicting the geothermal heat flux in Greenland: a machine learning approach*. Geophysical Research Letters, 44, 12271–12279. <https://doi.org/10.1002/2017GL075661>
- [31] Sandwell, D. T., Harper, H., Tozer, B., & Smith, W. H. (2021). *Gravity field recovery from geodetic altimeter missions*. Advances in Space Research, 68(2), 1059-1072. <https://doi.org/10.1016/j.asr.2019.09.011>

- [32] Siler, D. L., Pepin, J. D., Vesselinov, V. V., Mudunuru, M. K., & Ahmmed, B. (2021). *Machine learning to identify geologic factors associated with production in geothermal fields: A case-study using 3D geologic data, Brady geothermal field, Nevada*. Geothermal Energy, 9, 1-17. <https://doi.org/10.1186/s40517-021-00199-8>
- [33] Uieda, L., & Barbosa, V. C. (2017). *Fast nonlinear gravity inversion in spherical coordinates with application to the South American Moho*. Geophysical Journal International, 209(1), 162-176. <https://doi.org/10.1093/gji/ggw390>
- [34] Uyeda, S., & Watanabe, T. (1970). *Preliminary report of terrestrial heat flow study in the South American continent; distribution of geothermal gradients*. Tectonophysics, 10(1-3), 235-242. [https://doi.org/10.1016/0040-1951\(70\)90109-5](https://doi.org/10.1016/0040-1951(70)90109-5)
- [35] Veloza, G., Styron, R., Taylor, M., & Mora, A. (2012). *Open-source archive of active faults for northwest South America*. GSA Today, 22(10), 4-10. <https://doi.org/10.1130/GSAT-G156A.1>